3 Testing My Code

I have developed a code with periodic boundary conditions in order to allow benchmarking comparisons to be made with XES1. I have also made a code capable of simulating the behaviour of a floating wall in front of a plasma. The floating case is very similar to the type of problem I will encounter whilst simulating probe behaviour. The periodic results will be discussed first before moving on to the floating case.

3.0.5 Cold Plasma Oscillations

It is well known that if electrons in a plasma are displaced from their equilibrium position they will feel a restoring force due to electric fields which will act to quickly return the electrons to their equilibrium position. Once they reach this equilibrium position their kinetic energy will cause the electrons to overshoot and so a cycle begins with electrons oscillating around their respective equilibrium positions. The time frequency at which these oscillations occur is called the plasma frequency (ω_p). This is related to fundamental plasma parameters as

$$\omega_p = \frac{n_e m}{q^2 \epsilon_0} \tag{20}$$

In a real plasma these oscillations are non-dispersive, the frequency the electrons will oscillate at is always the plasma frequency and does not depend on the initial amplitude or wave number of the displacement. This is not the case in a periodic PIC simulation of the plasma, alias effects from the grid introduce a dispersion relation. The frequency the electrons will oscillate at now has a wave number dependence [12]

$$\omega(k) = \omega_p cos\left(\frac{k\Delta x}{2}\right) \tag{21}$$

$\omega(k)$ is the frequency that will be measured in PIC experiments. It is possible to measure this by plotting the kinetic energy of the electrons against time. As a first test a plot was made of kinetic energy and potential energy against time.

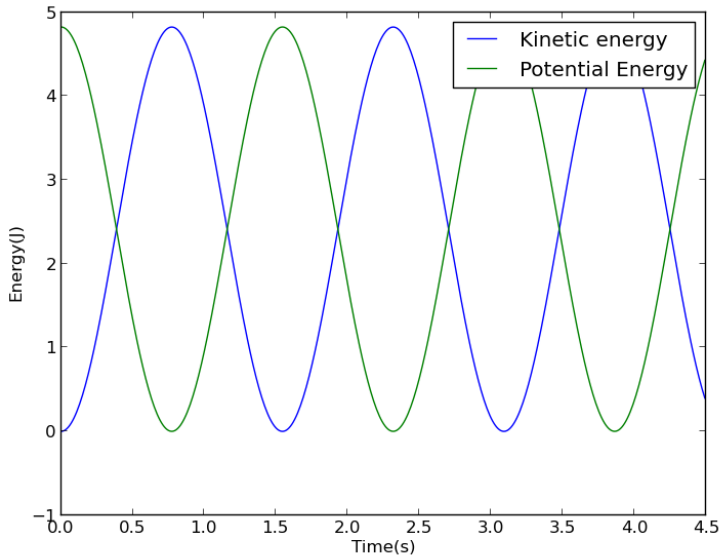

Figure 8: A plot of Kinetic energy and Potential Energy versus time. Shows the interchange of kinetic energy with potential energy

The electrons begin stationary with no kinetic energy. Their displacement gives them a potential energy which is converted into kinetic energy. The velocity has a sinusoidal dependence of time, the kinetic energy (τ) therefore obeys

$$\tau = Asin^2(\omega_p t) \tag{22}$$

where A is the amplitude. By fitting this curve to the plot of kinetic energy it is possible to determine ω_p. This can be carried out for multiple wave numbers to see if the plasma frequency does have a mode dependence.

The code was set up with the following parameters. The code was ran with different

L	2π
GP	512
N	1024
W	1e6

modes ranging from 1 to 70. The plasma frequency was measured for each and the results are shown below along with the theoretical dispersion relation.

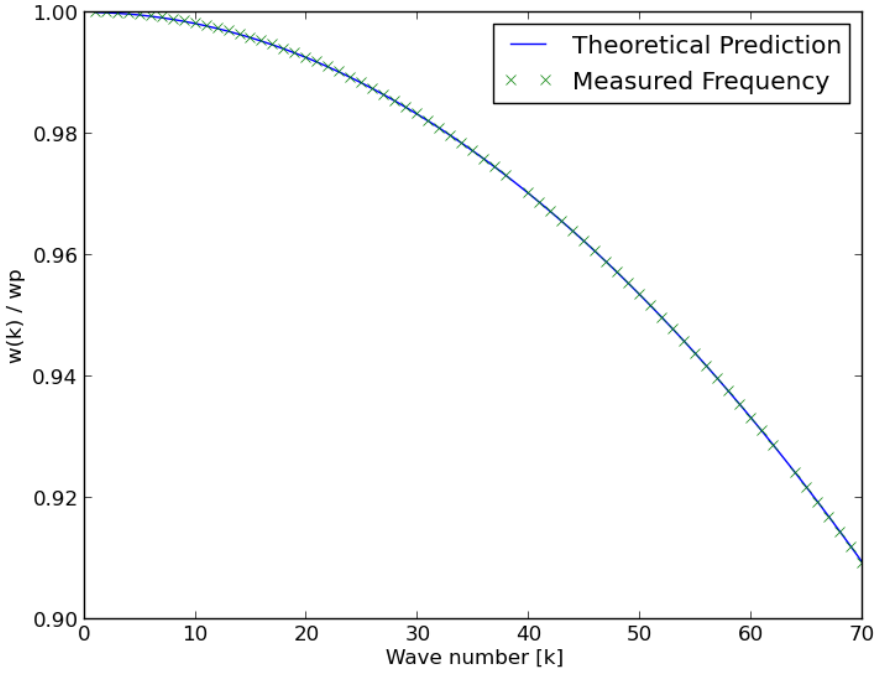

Figure 9: Dispersion Relation for the cold plasma oscillations both measured and theoretical

The two are in good agreement with each other thus demonstrating the aliasing effects of the grid.

3.0.6 Cold Beam Instability

The cold beam instability is another phenomenon found to occur in periodic PIC codes but in reality the system is stable. It is again caused by an aliasing effect from the grid. During this instability an initially cold beam of electrons will heat up until a saturation temperature is reached, at which point the instability is quenched. The electrons are initially given a uniform drift velocity v_0 and are uniformly distributed throughout the grid. The instability leads to an increase in thermal energy of the particles but not at an expense of their initial kinetic energy, as a result the total energy of the system increases due to this instability which is a non-physical result. Theory predicts the instability will stop once

$$\frac{\Lambda_D}{\Delta x} = \frac{v_t}{w_p \Delta x} \approx 0.046 \tag{23}$$

The effects of the instability are shown below.

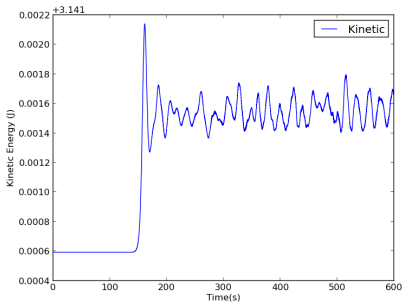

Figure 10: The kinetic energy of the simulation increases with time until the instability saturates.

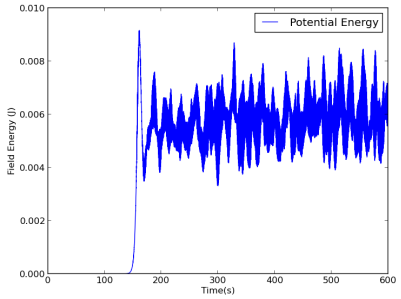

Figure 11: The potential energy of the simulation also increases with time until the instability saturates.

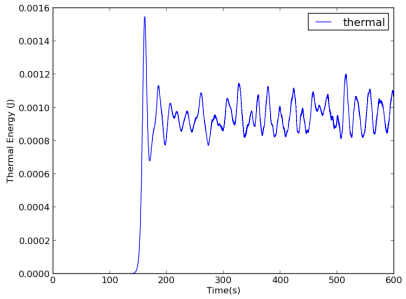

Figure 12: The beam gains thermal energy due to the cold beam instability. The instability saturates once the beam has warmed sufficiently

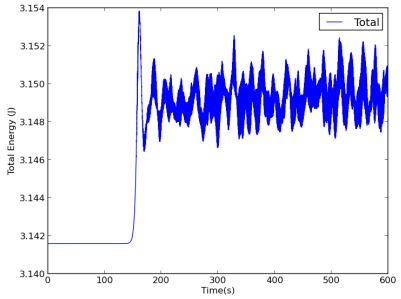

Figure 13: The instability leads to an unphysical source of energy, it is not the initial drift energy that is converted into thermal energy.

The thermal energy of the beam rises until a critical temperature has been reached, at that point the instability abruptly stops and energy fluctuates but does not grow. To test the point of saturation simulations were run with my code keeping the length of the system the same but varying the number of grid points which is equivalent to changing Δx. In all runs the length of the system was 2π and the same number of particles were used with the same initial velocity. The thermal energy at saturation was used to determine the thermal velocity and this was then compared to (23). A coefficient of 0.049 was found to be the average result which is consistent with Berkley's XES1 code. The relation is an approximate one. Tests were also carried out on how the initial velocity of the electrons affected the thermal velocity at saturation, it was found not to have an effect which is consistent with theory.

As the instability stops once the temperature has reached thousandths of an eV it is not likely that this instability will cause any problems in simulations that I will be doing, never the less this instability provided a useful test case on which to benchmark my code. Giving

a temperature to the beam at the beginning of the simulation prevents the instability from occurring provided the beam temperature is higher than the saturation temperature.

3.0.7 Two Stream Instability

This is a classic test case for a PIC code. The code is set up with two streams of electrons moving in opposite directions through a neutralising ion background. The beams are perturbed to give a sinusoidal density perturbation. The density perturbation in one beam reinforces the density perturbation in the other beam and vice versa. This leads to an exponential rate of growth for the instability. The initial drift energy of the electrons is converted into electric field energy which then acts to scatter the particles in phase space. As a result the temperature of the beams rises. The particles become trapped in vortices.

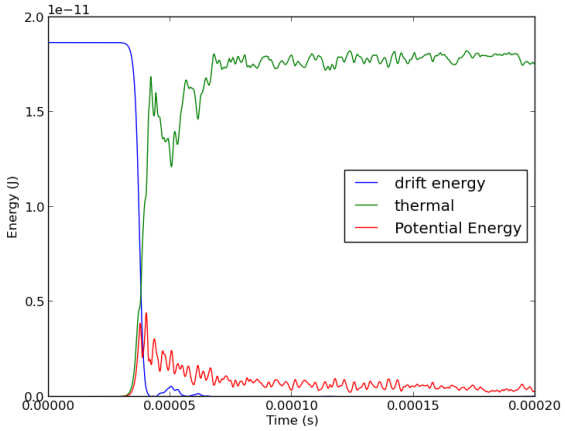

Figure 14: The initial drift energy of the beam is converted into thermal energy

The vortices are shown in the phase space plots below.

3.0.8 Floating Wall

To make the transition from a periodic code which models an infinite plasma to a finite plasma with boundaries on either side required changing the matrix solver and adding boundary conditions. By testing my periodic code I have established every part of the code apart from the matrix solver is in working order. The matrix solver used in my code is the one provided by Numerical Recipes [15]. It has been benchmarked with test cases to ensure it is working correctly so I can be confident my code works as it should do. Another test of the matrix solver was the observation of a self-force, the phenomenon of a particle depositing charge on the grid and then feeling a force from that charge. This was something I investigated because it had been observed in my code but a lot of literature claims it should not exist [12] [17]. This turns out to only be the case for a periodic code and not one with boundary conditions which is misleading. More details of the self-force can be found in the appendix.

In the floating test case a source of plasma is on the left hand side of the domain and on the right is a wall that collects the charged particles hitting it. The domain is initially filled

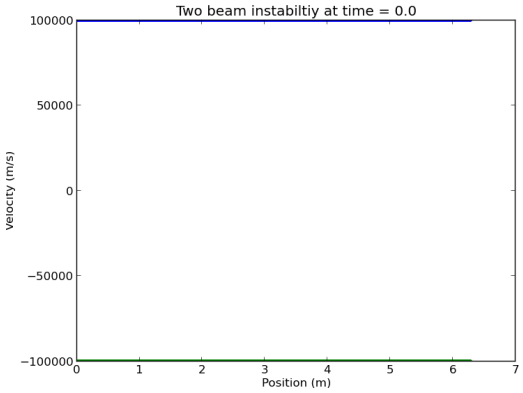

Figure 15: Two cold beams with velocity in opposite directions.

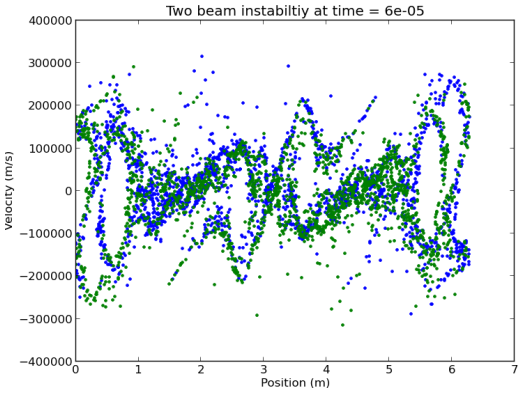

Figure 16: Vortices form and particles begin to move backwards.

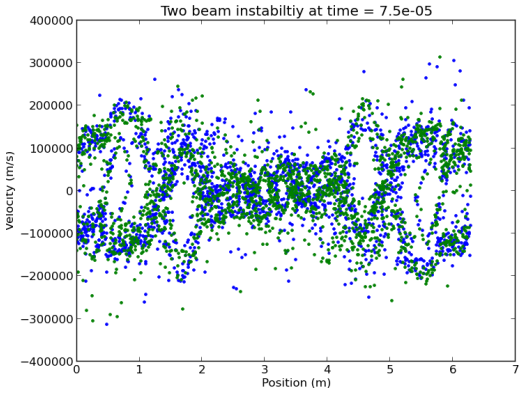

Figure 17: Some particles gain energy up to three times their initial kinetic energy

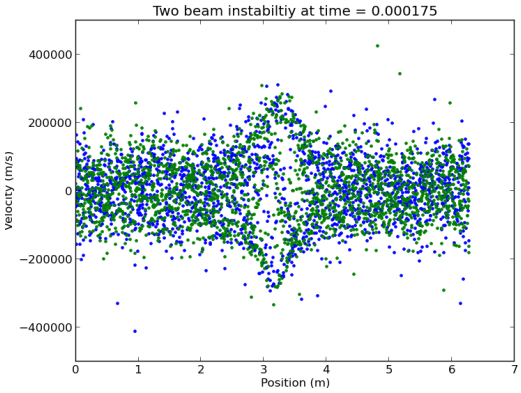

Figure 18: The vortices eventually merge into one.

with a uniform, neutral plasma with a temperature as specified by the user. It is possible to give the ions and electrons a different temperature. The electrons are much more mobile due to their lighter mass than the ions and so the wall quickly becomes negatively charged. This accelerates ions towards the wall and retards the flow of electrons and leads to the formation of a positive sheath in front of the wall as seen in experimental plasmas [18]. At each time step equal numbers of ions and electrons are injected as pairs in the same location with a velocity sampled from a Maxwellian distribution. Injecting the particles as pairs i.e. at the same location prevents the generation of non-physical electric fields in the source region.

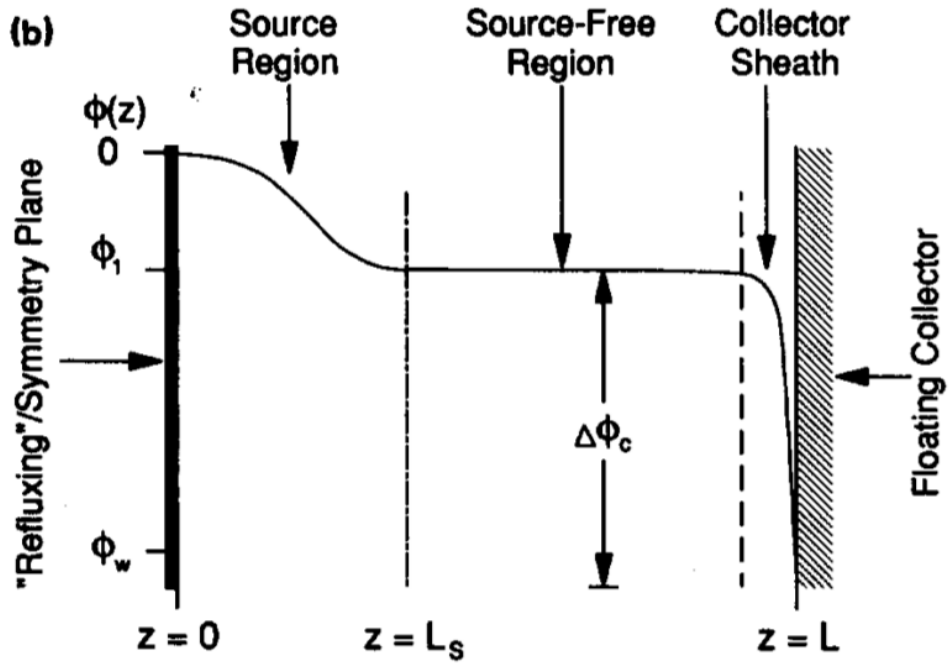

Figure 19: A diagram representing the domain in the floating case. Particles are injected as pairs in the source region and travel to the wall located on the right hand side. [19]

Tests were carried out to ensure the distribution of velocities is truly Maxwellian.

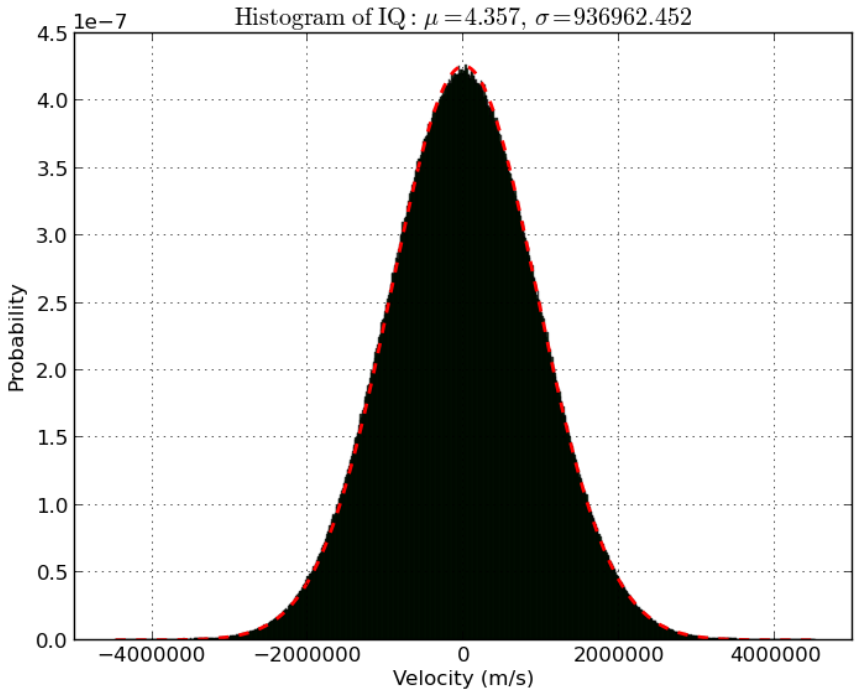

Figure 20: The initial distribution of velocity for the electrons at 5eV.

The electrons were given a temperature of 5eV. The resulting velocity distribution has a velocity centred around zero and a standard deviation equivalent to the thermal velocity as expected. Particles that travel across the domain and hit the wall deposit their charge on to the wall and are then deleted from the system. Particles that exit from the left hand side are refluxed. This means they are given a new velocity towards the wall sampled from a Maxwellian distribution. The idea behind this is that the source region in the code represents only a fraction of the actual source region as this will be much larger than what it is possible to simulate within a reasonable time for a PIC code. So particles that exit the domain are replaced by thermal particles travelling in the opposite direction. It is possible to reflect the particles that hit the left hand boundary rather than generate a new velocity for them, however without collisions in the model electrons that are reflected from the sheath in front of the wall become trapped in the system with a reflecting boundary on the left hand side. Refluxing provides a way to rethermalise these electrons as collisions would do.

A problem encountered with this test case is a loss of temperature in the source region. The source is initially filled with a uniform plasma at the desired temperature. However the more energetic particles quickly leave the source region and travel to the wall leaving the slower moving particles behind, lowering the temperature of the source region. The source region loses the high end energy tail of the distribution and becomes non-Maxwellian over time. Although there is a constant source of new particles it is far more likely that the new particles will be moving at a slower speed due to the nature of a Maxwellian distribution. These slow moving particles then take longer to exit the source region. This is a direct result of simulating only a small source region. To confirm that this was the source of the error and

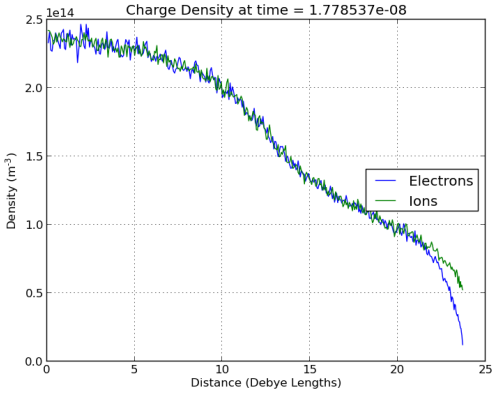

Figure 21: A positive sheath with a thickness of a few Debye length forms in front of the wall and shields the rest of the plasma from the negative charge.

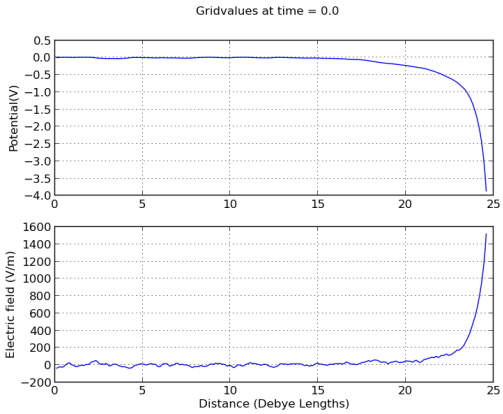

Figure 22: The electric field is zero everywhere in the quasi-neutral plasma but rapidly increases in the sheath region. This field acts to accelerate ions in the sheath and de-accelerate electrons.

not an inherent problem in the code a test case was run in which both sides of the domain reflected particles that reached it. No particles were added to or lost from the system. In this case the temperature of the particles was the same at all times. Attempts have been made to conserve the temperature in the floating case, firstly by adding binary collisions which helps but does not remove the problem as the fast particles will still quickly escape. Other attempts involved artificially changing the velocity of all particles in the source region at a set number of time steps. Adding this feature generated electric fields in the source region which led to a rapid breakdown of the simulation. Despite this difficulty the code does exhibit physical results such as the generation of a positive sheath a few Debye lenghs wide in front of the wall and zero electric field everywhere except from the source region. These results are shown in figure 21 and 22. The wall reaches a floating potential that oscillates with time. Because of the loss of temperature it is not possible to compare the floating potential with that predicted by Stangeby [8] as this assumes a Maxwellian distribution at all times. The loss of temperature has been documented in other codes, their solution is usually to limit the time duration of the simulation to reduce the effect. Other codes such as BIT1 do manage to conserve temperature and this is a feature I will be looking for in my final code [20].

4 Future plans

As well as developing my own code I have also produced an extensive report discussing the PIC algorithm in detail and giving more detail into the interpretation of probes. This report will form a solid basis for an introductory chapter(s) to my thesis. My code has been tested and benchmarked against the well established XES1 code so I can be confident in the reliability of my code. The next step is to identify a 3d-3v code for use in the rest of my project. The code I have developed will provide a useful test bed to explore the effects of

adding new physics before implementing it into the 3d code. A detailed plan is shown in the gantt chart below.

	Task	Assigned To	Start	End	Dur	%
			26/11/14	1/6/15	127	
1	Identify 3d-3v PIC code		26/11/14	31/12/14	24	
2	Install Code, Read Documentation		1/1/15	1/2/15	21	
3	Run test cases with new Code		1/1/15	1/2/15	21	
4	Identify Missing Physicsa		1/1/15	1/2/15	21	
5	Run Simple LP test cases (1D-2D)		1/2/15	1/4/15	43	
6	Implement Missing Physics		1/3/15	1/6/15	62	
7	Run Simple Test Caes (3D)		1/4/15	1/5/15	21	
8	Comparison of Results with theory		1/5/15	1/6/15	20	

Implementing missing physics from the code will be an ongoing part of my project. During this period I will also study the effects of this additional physics on Langmuir Probe data.

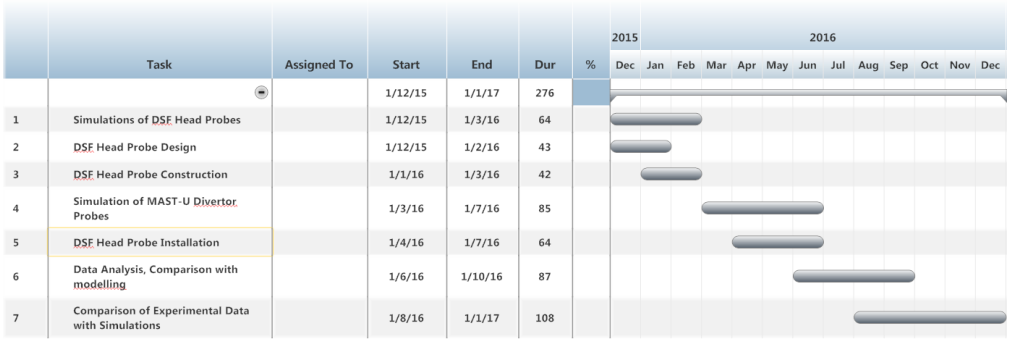

	Task	Assigned To	Start	End	Dur	%
			1/12/15	1/1/17	276	
1	Simulations of DSF Head Probes		1/12/15	1/3/16	64	
2	DSF Head Probe Design		1/12/15	1/2/16	43	
3	DSF Head Probe Construction		1/1/16	1/3/16	42	
4	Simulation of MAST-U Divertor Probes		1/3/16	1/7/16	85	
5	DSF Head Probe Installation		1/4/16	1/7/16	64	
6	Data Analysis, Comparison with modelling		1/6/16	1/10/16	87	
7	Comparison of Experimental Data with Simulations		1/8/16	1/1/17	108	

The remainder of the time is scheduled for writing up.

5 Appendix

5.1 Self Force

The presence of the spatial grid introduces some non-physics into the simulation, an example of which is the self force. The self force is the name given to the phenomenon in which a charged particle becomes aware of its own field and so repels itself. This non-physical force is inherent in any system that uses the spatial grid to work out charge density and electric field values. Imagine a charged particle placed in between two grid points, let the particle reside closer to the left grid point to begin with. Using the first order weighting scheme (CIC) the particle will deposit more of its charge on to the left grid point than it will on to the right. This density will then be used to work out a potential and finally a field which is then interpolated back to the particles position, not necessarily using the same weighting scheme but for now consider it is the same. The particle will feel a larger force from the grid point on its left than it will do from the grid point on its right due to the relative distances and as a result it will be repelled from the left grid point and head towards the right. Although this argument assumed a first order weighting scheme, the self force is present with any method of weighting. It is possible to prove that the self force is introduced by the addition of a spatial grid rather than from any approximations made in using finite difference methods to solve Poissons equation. The following method is adapted from the textbook 'Numerical particle-in-cell Methods: Theory and Applications' [21].

The electric potential due to a point charge with charge q at a distance r is given by

$$\psi = \frac{1}{4\pi\epsilon_0}\frac{q}{r} = \frac{Cq}{r} \tag{24}$$

where C is a constant. Now introduce a spatial grid with spacing dx. Let the particle be a distance r from the grid point on the left and so a distance $dx - r$ from the point on the right. The particle will deposit a charge ρ_1 on the left grid point and a charge ρ_2 on the right where

$$\rho_1 = q\frac{(dx - r)}{dx} \tag{25}$$

and

$$\rho_2 = q\frac{r}{dx} \tag{26}$$

The particle will feel a potential that is a combination of the potential from the two grid points. From (24)the potential at the particle is

$$\frac{Cq}{dx}\left(\frac{dx - r}{r} + \frac{r}{dx - r}\right) \tag{27}$$

The force at the particle is given by

$$F = -\frac{\partial\psi}{\partial r}q = Cq^2 dx\frac{dx - 2r}{r^2(dx - r)^2} \tag{28}$$

Despite the potential and electric field having been solved exactly without finite difference methods there still exists a self force due to the introduction of a spatial grid. This force is

zero if the particle is at the midpoint of a cell ($r = \frac{dx}{2}$) and acts to repel the particle from its closest grid point.

It is possible to quantify this force in the case of a complete PIC simulation where FDM are used. As before Poisson's equation is discretised

$$-\rho_J = \frac{\psi_{J+1} - 2\psi_J + \psi_{J-1}}{(dx)^2} \tag{29}$$

This equation can be solved analytically without a matrix equation.

$$\psi_J = \frac{I-J}{I}A + \frac{J}{I}B + \frac{dx^2}{I}\left[(I-J)\sum_{k=1}^{J} k\rho_k + J\sum_{k=J+1}^{I-1}(I-k)\rho_k\right] \tag{30}$$

Where I is the number of the grid cells , A is the potential at the left hand side boundary and B the potential at the right hand side. This will now be carried out for one particle. Let the particle lie between grid points $x_{\alpha-1}$ and x_α at position x. The offset (σ) is given by

$$\sigma = \frac{x - x_{\alpha-1}}{dx} \tag{31}$$

Using (30) it is possible to calculate the potential at the grid points either side of the particle.

$$\psi_\alpha = \frac{I-\alpha}{I}A + \frac{\alpha}{I}B - \frac{dx^2}{I}(I-\alpha)\left[(\alpha-1)\rho_{\alpha-1} + \alpha\rho_\alpha\right] \tag{32}$$

$$\psi_{\alpha-1} = \frac{I-\alpha+1}{I}A + \frac{\alpha-1}{I}B - \frac{dx^2}{I}(\alpha-1)\left[(I-\alpha+1)\rho_{\alpha-1} + (I-\alpha)\rho_\alpha\right] \tag{33}$$

Similar expressions can be derived for $\psi_{\alpha+1}$ and $\psi_{\alpha-2}$. These can then be used to derive the value of the electric field at the adjacent grid points.

$$E_\alpha = \frac{\psi_{\alpha-1} - \psi_{\alpha+1}}{2dx} = \frac{A-B}{Idx} - \frac{dx}{I}\left[(\alpha-1)\rho_{\alpha-1} + (\alpha - \frac{I}{2})\rho_\alpha\right] \tag{34}$$

$$E_{\alpha-1} = \frac{\psi_{\alpha-2} - \psi_\alpha}{2dx} = \frac{A-B}{Idx} - \frac{dx}{I}\left[(\alpha - \frac{I}{2} - 1)\rho_{\alpha-1} + (\alpha - I)\rho_\alpha\right] \tag{35}$$

Using the first order weighting method, the force at the particle E_i will be given by

$$E_i = E_{\alpha-1}(1-\sigma) + \sigma E_\alpha = \frac{A-B}{Idx} - \frac{dx}{I}\left[(\alpha - \frac{I}{2} - 1 + \frac{I}{2}\sigma)\rho_{\alpha-1} + (\alpha - I + \frac{I}{2}\sigma)\rho_\alpha\right] \tag{36}$$

The self force is inherent in PIC codes and always acts to repel a particle from its nearest grid point going to zero when the particle is at the midpoint of a grid cell. Interestingly this equation shows the impact that boundary conditions have on the self force. The force not only depends on the location of the particle in the grid cell but also in which cell it lies in. Provided there are sufficient amount of particles the self force will be negligible.

6 References

References

[1] E. V. Shun'ko, *Langmuir Probe in Theory and Practise*, 1st ed. Universal Publishers, 2009.

[2] R. D. Monk, "Langmuir probe measurements in the divertor plasma of the jet tokamak," 1996.

[3] I. G. Brown, A. B. Compher, and W. B. Kunkel, "Response of a langmuir probe in a strong magnetic field," *Physics of Fluids (1958-1988)*, vol. 14, no. 7, 1971.

[4] P. C. Stangeby, G. M. McCracken, S. K. Erents, and G. Matthews, "DITE Langmuir probe results showing probesize and limitershadow effects," *Journal of Vacuum Science & Technology A*, vol. 2, no. 2, 1984.

[5] P. C. Stangeby, J. D. Elder, J. A. Boedo, B. Bray, N. H. Brooks, M. E. Fenstermacher, M. Groth, R. C. Isler, L. L. Lao, S. Lisgo, G. D. Porter, D. Reiter, D. L. Rudakov, J. G. Watkins, W. P. west, and D. G. Whyte, "Interpretive modelling of simple-as-possible plasma discharges on DIII-D using the OEDGE code ," 2002.

[6] McGraw-Hill, "The characteristics of electrical discharges in magnetic fields," *National nuclear energy series*, vol. 5, 1949.

[7] G. F. Matthews, "Tokamak plasma diagnosis by electrical probes," *Plasma Physics and Controlled Fusion*, vol. 36, no. 10, p. 1595, 1994. [Online]. Available: http://stacks.iop.org/0741-3335/36/i=10/a=002

[8] P. C. Stangeby, *The Plasma Boundary of Magnetic Fusion Devices*. IoP, 2000.

[9] G. F. Matthews, S. J. Fielding, G. M. McCracken, C. S. Pitcher, P. C. Stangeby, and M. Ulrickson, "Investigation of the fluxes to a surface at grazing angles of incidence in the tokamak boundary," *Plasma Physics and Controlled Fusion*, vol. 32, no. 14, p. 1301, 2004. [Online]. Available: http://stacks.iop.org/0741-3335/32/i=14/a=004

[10] M. Komm, R. Dejarnac, J. P. Gunn, and Z. Pekarek, "Three-dimensional particle-in-cell simulations of gap crossings in castellated plasma-facing components in tokamaks," *Plasma Physics and Controlled Fusion*, vol. 55, no. 2, p. 25006, 2013. [Online]. Available: http://stacks.iop.org/0741-3335/55/i=2/a=025006

[11] "Advanced probes for edge plasma diagnostics on the CASTOR tokamak," *Journal of Physics: Conference Series*, vol. 63, no. 1, p. 12001, 2007. [Online]. Available: http://stacks.iop.org/1742-6596/63/i=1/a=012001

[12] C. K. Birdsall and A. B. Langdon, *Plasma physics via computer simulation*, ser. Series in plasma physics. New York: Taylor & Francis, 2005, originally published: New York ; London : McGraw-Hill, 1985. [Online]. Available: http://opac.inria.fr/record=b1121477

[13] P. Hughes, *Particle-in-cell simulation of nonlinear plasma instabilities.* Dept of Physics and Astronomy The University of Manchester, 2007.

[14] http://www.daniel-martin.co.uk/files/pic.pdf.

[15] W. H. Press, S. A. Teukolsky, W. T. Vetterling, and B. P. Flannery, *Numerical Recipes in C (2Nd Ed.): The Art of Scientific Computing.* New York, NY, USA: Cambridge University Press, 1992.

[16] http://wwwnew.cs.princeton.edu/courses/archive/spring04/cos590/Stone/Lecture2.ppt.

[17] R. W. Hockney and J. W. Eastwood, *Computer Simulation Using Particles*, Hockney, R.˜W.˜& Eastwood, J.˜W., Ed. New York: McGraw-Hill, 1981. [Online]. Available: http://adsabs.harvard.edu/cgi-bin/nph-bib_query?bibcode=1981csup.book.....H

[18] K.-U. Riemann, "The bohm criterion and sheath formation," *J.Phys.D:Appl.Phys.*

[19] R. J. Procassini, C. K. Birdsall, and E. C. Morse, "A fully kinetic, selfconsistent particle simulation model of the collisionless plasmasheath region," *Physics of Fluids B: Plasma Physics (1989-1993)*, vol. 2, no. 12, 1990.

[20] D. Tskhakaya and S. Kuhn, "Effect of E B Drift on the Plasma Flow at the Magnetic Presheath Entrance," *Contributions to Plasma Physics*, vol. 42, no. 2-4, pp. 302–308, 2002. [Online]. Available: http://dx.doi.org/10.1002/1521-3986(200204)42:2/4⟨302::AID-CTPP302⟩3.0.CO;2-K

[21] N. Grigorev, Y. N. Grigoryev, V. A. Vshivkov, and M. P. Fedoruk, *Numerical "particle-in-cell" Methods: Theory and Applications*, ser. Theory and Applications. VSP, 2002. [Online]. Available: http://books.google.co.uk/books?id=cqbpONpHLDsC